NanoSIMS analysis of arsenic and selenium in cereal grain

Katie L. Moore[1], Markus Schröder[1], Enzo Lombi[2,3], Fang-Jie Zhao[4], Steve P. McGrath[4], Malcolm J. Hawkesford[4], Peter R. Shewry[4] and Chris R. M. Grovenor[1]

[1]Department of Materials, University of Oxford, Parks Road, Oxford OX1 3PH, UK; [2]Department of Agricultural Science, Faculty of Life Science, University of Copenhagen, Thorvaldsensvej 40, 1871 Frederiksberg C, Denmark; [3]Centre for Environmental Risk Assessment and Remediation, University of South Australia, Building X, Mawson Lakes Campus Mawson Lakes, South Australia, SA-5095 Australia and CRC CARE, PO Box 486, Salisbury, South Australia 5106, Australia; [4]Rothamsted Research, Harpenden, Hertfordshire AL5 2JQ, UK

Author for correspondence:
Katie L. Moore
Tel: +44 (0)1865 273766
Email: katie.moore@materials.ox.ac.uk

Received: *31 July 2009*
Accepted: *13 September 2009*

New Phytologist (2010) **185**: 434–445
doi: 10.1111/j.1469-8137.2009.03071.x

Key words: arsenic (As), cereal, NanoSIMS, rice (*Oryza sativa*), secondary ion mass spectrometry (SIMS), selenium (Se), subcellular localization, wheat (*Triticum aestivum*).

Summary

• Cereals are an important source of selenium (Se) to humans and many people have inadequate intakes of this essential trace element. Conversely, arsenic (As) is toxic and may accumulate in rice grain at levels that pose a health risk. Knowledge of the localization of selenium and arsenic within the cereal grain will aid understanding of their deposition patterns and the impact of processes such as milling.

• High-resolution secondary ion mass spectrometry (NanoSIMS) was used to determine the localization of Se in wheat (*Triticum aestivum*) and As in rice (*Oryza sativa*). Combined synchrotron X-ray fluorescence (S-XRF) and NanoSIMS analysis utilized the strengths of both techniques.

• Selenium was concentrated in the protein surrounding the starch granules in the starchy endosperm cells and more homogeneously distributed in the aleurone cells but with Se-rich hotspots. Arsenic was concentrated in the subaleurone endosperm cells in association with the protein matrix rather than in the aleurone cells. NanoSIMS indicated that the high intensity of As identified in the S-XRF image was localized in micron-sized hotspots near the ovular vascular trace and nucellar projection.

• This is the first study showing subcellular localization in grain samples containing parts per million concentrations of Se and As. There is good quantitative agreement between NanoSIMS and S-XRF.

Introduction

Selenium (Se) is an important trace element in the human diet (Schwarz & Foltz, 1957) and is a vitally important part of the enzyme glutathione peroxidase, which prevents tissue degeneration by acting as an antioxidant (Fordyce *et al.*, 2000; Hartikainen, 2005). It has been estimated that between 0.5 and 1 billion people world-wide may be deficient in Se, and this includes populations in developed countries (Combs, 2001). The recommended reference intake of Se in the UK is 60 μg d^{-1} for women and 75 μg d^{-1} for men (Broadley *et al.*, 2006) but in 1999 the intake was estimated to be as low as 35 μg d^{-1}, significantly below the reference intake (Rayman, 2002). This decrease has been attributed to a number of causes, most notably a reduction in the amount of wheat imported from North America, which has a higher Se content than European wheat (Hawkesford & Zhao, 2007). The Se content of wheat can be increased by applying an Se fertilizer to the soil as practised in Finland since the early 1980s (Eurola *et al.*, 1991).

Arsenic (As) is a carcinogenic and toxic element. Arsenic-contaminated groundwater is widely used for irrigating crops in Bangladesh and West Bengal, India, in particular for deliberate flooding of rice paddies. Rice (*Oryza sativa*) is one of the main foods in As-epidemic areas (Rahman *et al.*, 2008) and in Bangladesh makes up 73% of the calorific intake (Meharg & Rahman, 2003). Irrigation with As-contaminated water has resulted in rice with elevated concentrations of As, and surveys have shown that rice is a major

source of inorganic As (the most toxic form of As) in a rice-based diet (Williams *et al.*, 2007). Compared with other cereal crops, rice accumulates more As because of a higher bioavailability in the flooded paddy soil (Xu *et al.*, 2008), and also because arsenite is taken up by silicon transporters which are highly expressed in rice roots (Ma *et al.*, 2008).

To date there have been few reports of the location of As and Se in cereals at high resolution. This information is needed to understand how these trace elements are transported to and deposited in the grain, and whether milling will increase or minimize their concentrations. Most chemical analyses of trace elements in crops are performed using techniques that have high elemental sensitivity but do not have the necessary resolution to map the position of these elements at the subcellular scale, and in many cases require the whole grain to be milled and digested, hence losing spatial information altogether. Analytical techniques such as energy or wavelength dispersive X-ray spectroscopy have a resolution of *c.* 1 μm but do not have the necessary sensitivity to detect parts per million (ppm) concentrations. Spatially resolved X-ray absorption near edge structure (μ-XANES) and synchrotron-based X-ray fluorescence (S-XRF) techniques (Meharg *et al.*, 2008) have very high sensitivities and a resolution of a few microns, which allows mapping of the whole grain but generally cannot resolve subcellular features. Meharg *et al.* (2008) present S-XRF images showing As distribution in fractured rice grains and found As to be 'preferentially localised at the surface, in the region corresponding to the pericarp and aleurone layer'. However, a subsequent study (Lombi *et al.*, 2009) investigating As distribution in thin sections of rice grains indicated that high concentrations were present in the aleurone and outer parts of the endosperm near the ovular vascular trace. Lyons *et al.* (2005a) showed that Se was concentrated in wheat grain embryos prepared by hand dissection but also evenly distributed throughout the whole grain, in comparison to other mineral nutrients (e.g. zinc (Zn), iron (Fe) and potassium (K)) which were concentrated in the aleurone. Williams *et al.* (2009), using S-XRF, showed a similar accumulation pattern of Se in rice grains with enrichment in the embryo and a concentration gradient decreasing from the outer parts of the grain to the centre.

Secondary ion mass spectrometry (SIMS) microscopy is a technique well suited for analysing the distribution of trace elements at high resolution. SIMS is increasingly being used to analyse biological materials as it is recognized that this technique has excellent potential for trace element analysis because of its unique combination of high sensitivity, high lateral resolution, detectability of all elements and isotopes, molecular imaging and the potential for 3D analysis (Burns, 1982; Chandra *et al.*, 2000; Guerquin-Kern *et al.*, 2005). The NanoSIMS has been specifically designed for high-resolution, high-sensitivity SIMS analysis with particular focus on biological, materials and geological applications (http://www.cameca.fr/html/product_nanosims.html). In all analytical instruments there is a trade-off between sensitivity and resolution, and the NanoSIMS does not offer the sensitivity of techniques such as S-XRF or the lateral resolution of transmission electron microscopy with energy dispersive X-ray spectroscopy (TEM + EDX); however, it is the combination of high sensitivity (down to ppm) and high lateral resolution (down to 50 nm) that makes this technique ideally suited to analyse trace elements in biological materials.

NanoSIMS analysis has been successfully applied to several biological systems; for instance by Quintana *et al.* (2006) to study ferritin and hemosiderin cores from the brains of Alzheimer patients, and to study the nickel (Ni) distribution in the hyperaccumulator plant *Alyssum lesbiacum* (Smart *et al.*, 2007). Audinot *et al.* (2004) used NanoSIMS to image traces of As in human hair and showed that the high lateral resolution obtainable prevents any misinterpretation of whether the As detected by conventional chemical analysis techniques (atomic absorption or chemical analyses) results from external contamination or from physiological absorption by the patient. These samples are similar to the cereal grain samples analysed in this paper in the sense that sample preparation was relatively simple as the starting materials contain little free water and therefore do not require complex preparation methods (Chandra & Morrison, 1992).

In the present study, the localization of As in rice and Se in wheat (*Triticum aestivum*) has been investigated using high-resolution NanoSIMS analysis. The localization patterns of As and Se were compared with those of their respective chemical analogues phosphorus (P) and sulphur (S).

Materials and Methods

Samples

Wheat (*Triticum aestivum* L. cv. Hereward) grain samples were obtained from a field experiment conducted in the University of Nottingham's (UK) experimental farm in 2007. Selenium fertilizer was applied to the crop at the stem extension stage in the form of sodium selenate (400 g Se ha^{-1}). Other inputs were the same as in normal agronomic practice. The wheat was harvested at maturity. Rice (*Oryza sativa* L. cv. Oochikara) grain samples were obtained from a pot experiment conducted in a glasshouse at Rothamsted Research (Harpenden, UK). Sodium arsenite (10 mg As kg^{-1} soil) was added to the soil at the beginning of the experiment and rice was grown under flooded conditions (Xu *et al.*, 2008). At maturity, rice grains were collected and dehusked, but not polished, so that the aleurone layer was intact. In both experiments high concentrations of Se and As were achieved in the grains by the addition of Se or As to the soil to ensure that they would be well above the sensitivity limit for NanoSIMS analysis. These

concentrations were measured using inductively-coupled plasma mass-spectroscopy (ICP-MS) (Agilent LC1100 series and Agilent ICP-MS 7500ce; Agilent Technologies, Santa Clara, CA, USA) after an acid digestion (HNO_3 – H_2O_2) in a microwave digester, and were found to be 16.7 mg kg^{-1} Se in the wheat samples and 2.5 mg kg^{-1} As in rice. The wheat plants showed no obvious signs of suffering from Se toxicity even with this high concentration. The bulk concentration of As in the rice at 2.5 mg kg^{-1} was rather similar to the highest concentrations (1.7 mg kg^{-1}) measured in rice grains collected from As-contaminated fields in Bangladesh by Meharg & Rahman (2003).

Sample preparation

As cereal grain samples contain little water at maturity, conventional SIMS preparation procedures (Burns, 1982; Chandra & Morrison, 1992; Grovenor *et al.*, 2006) to remove water from biological samples before analysis under ultra high vacuum were not necessary. However, as rice grains readily absorb water on storage, it was necessary to keep them under a vacuum of *c.* 10^{-2} mbar for 1 wk before mounting to remove the majority of the residual water. Whole-grain samples were mounted in London Resin White (London Resin Company, Basingstoke, UK) in 10-mm-diameter steel rings which fit into the NanoSIMS holders. No fixation or embedding was performed; the resin simply located the grain in the ring. Half of each type of grain was left protruding from the top of the ring and, to create a flat surface for analysis, a razor blade was used to transversely section the protruding grain level with the top of the holder. Results from two rice grains and two wheat grains are presented here, but analyses were performed on several other samples of both types of grain with very similar results.

Samples were examined by conventional and confocal light microscopy and by scanning electron microscopy (SEM) to identify flat regions for SIMS analysis. Samples were then coated with 10 nm of platinum to prevent charging during SIMS analysis.

To ensure that artefacts had not been introduced by the above sample preparation method, one immature wheat grain sample was prepared by high-pressure freezing as a comparison. This sample (16 d post-anthesis) was obtained from a pot-grown wheat plant without Se fertilization and contained little Se (i.e. below the detection limit for the NanoSIMS). The grain sample was frozen using pressurized jets of liquid nitrogen. High-pressure freezing was able to prevent the redistribution of diffusible ions that can occur during desiccation of samples with a high water content, and damage to the sample by the growth of ice crystals. This sample was post-stained with osmium tetroxide and embedded in Spurr's resin. Sections 1 μm thick were cut with a Reichert ultratome (Reichert, Vienna, Austria), placed onto a 7 mm × 7 mm silicon wafer and gently warmed to give good adherence to the silicon substrate. As the sections were thin it was not necessary to coat with platinum as the conductivity of the silicon substrate prevented charge build-up.

Analytical methods

SIMS analysis was performed using the CAMECA NanoSIMS 50 ion microprobe which allows simultaneous detection of five ionic species from the same sputtered volume with high mass and high spatial resolution while still maintaining up to 50% transmission of all the sputtered ions necessary to achieve high sensitivity (http://www.cameca.fr/html/product_nanosims.html). A focused 16-keV Cs^+ primary ion beam is scanned over the surface of the sample and the sputtered negative secondary ions are collected and analysed using a double focusing mass spectrometer. In this study, the instrument was generally configured to maximize the sensitivity to trace elements by using a large D1 aperture which reduced the lateral resolution to *c.* 100–200 nm but improved the counting statistics. Higher resolution images (10 μm × 10 μm maps) were taken with smaller D1 apertures and have a spatial resolution of better than 100 nm. The incident Cs^+ beam currents were 2–4 pA for all experiments unless otherwise stated. The region of interest was selected first with a charge-coupled device (CCD) camera and then using the secondary electron image created by scanning the primary ion beam. In all cases it was necessary to remove the platinum coating from the area of interest and implant caesium ions to achieve steady-state analysis conditions before collecting chemical images (Guerquin-Kern *et al.*, 2005). This was achieved by continued scanning of the region of interest with a large, defocused beam until no further changes in the secondary electron signal were observed and steady-state analysis conditions were reached. As the bulk concentrations of the elements of interest were low, it was necessary to carefully calibrate the detectors using appropriate standards to ensure correct tuning of the spectrometer. Sodium selenate, dissolved in water and re-crystallized onto a resin surface, was used for Se calibration and a solid gallium arsenide standard was used for As. Ion maps were collected simultaneously for $^{16}O^-$, $^{12}C^{14}N^-$, $^{32}S^-$, $^{31}P\ ^{16}O^-$ and $^{75}As^-$ or $^{80}Se^-$ together with the secondary electron map. Secondary electrons are produced during the sputtering process and these can be used to give an indication of both sample morphology and surface topography. NanoSIMS maps are presented in an arbitrary linear colour scale, with red and yellow regions indicating higher concentration and blue and black indicating lower concentration.

An FEI FIB 200 focused ion beam (FIB) microscope (FEI Company, Hillsboro, OR, USA) with a 30-keV Ga^+ primary ion beam with a current of 100–300 pA was used to simulate the effect of the NanoSIMS incident ion beam on the sample surface topography.

One rice grain sample was also analysed with synchrotron X-ray fluorescence (S-XRF) using beamline 20ID at the advanced photon source (APS) at Argonne National Laboratory (Argonne, IL, USA). This sample was mounted in resin and prepared as described above so that the same sample could be analysed with the NanoSIMS after S-XRF analysis. Half of the grain (3 mm × 1.7 mm) was mapped using S-XRF with a step size of 15 μm and the beam focused to *c.* 2 μm. The rationale for this experiment was suggested by previous work by Meharg *et al.* (2008) using S-XRF showing increased As concentrations near the surface of the grain in similar rice samples. Mapping large areas is very time consuming in the NanoSIMS, and therefore the analytical strengths of the two techniques have been combined by mapping a rice grain at lower resolution with S-XRF to target regions with high As content which were subsequently studied at higher spatial resolution in the NanoSIMS.

Results and Discussion

Selenium distribution in wheat grains

Figure 1 shows a scanning electron micrograph of an area of the wheat grain selected for NanoSIMS analysis. It shows the outer part of the endosperm, with a single layer of thick-walled aleurone cells surrounded by the outer layers of the grain (testa and pericarp) and enclosing the starchy endosperm cells. (The main morphological components of wheat grains are described in Grundas (2003).) The aleurone cells are clearly well preserved, with phytate granules being easily visible. The starchy endosperm cells contain starch granules, with the layer of cells immediately below the aleurone being particularly protein-rich (Tosi *et al.*, 2009). The surface, although not completely flat, is not so rough that reliable NanoSIMS analysis is prevented.

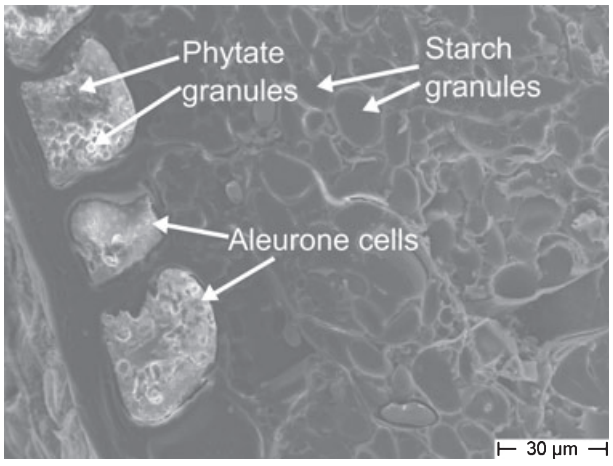

Fig. 1 Scanning electron micrograph of the outer edge of a wheat (*Triticum aestivum*) grain showing the aleurone layer (left) and the starchy endosperm (right). This area was subsequently analysed in the NanoSIMS.

Figure 2 shows NanoSIMS ion maps of the area shown in Fig. 1 taken with a dwell time of 60 ms per pixel and a current of 2 pA. Significant differences can be observed between the individual elemental maps, showing that the influence of topography does not dominate the local ion yield. This indicates that the images reveal genuine variations in composition. The $^{12}C^{14}N^-$ ion is commonly used in SIMS analysis of biological materials as a marker for the distribution of proteins (Levi-Setti, 1988) and to illustrate morphology (Grignon *et al.*, 1992). The $^{12}C^{14}N^-$ signal intensity in Fig. 2 is much stronger in the regions around the starch granules, which is consistent with the granules being surrounded with a protein-rich matrix. The oxygen map shows a more even distribution, apart from in the aleurone cells, where intense regions of signal are observed. These regions correspond with high intensity in the $^{31}P^{16}O^-$ map and show the location of the phytate granules. Although a bulk concentration of 16.7 mg kg^{-1} Se is very high for wheat grain (normal values lie within the range 0.01–2 mg kg^{-1} Se (Hawkesford & Zhao, 2007)), it still presents a serious analytical challenge for techniques with high spatial resolution. At this concentration, however, the $^{80}Se^-$ signal is readily detected by the NanoSIMS and is relatively uniformly distributed across the protein matrix of the aleurone cells but more concentrated in the region surrounding the starch granules in the starchy endosperm cells. These results are consistent with those of Eurola *et al.* (1991), who showed that flour fractions containing the aleurone cells contained only slightly higher Se concentrations than flours that did not. They also agree with the results of Lyons *et al.* (2005a), who showed that the concentration of Se in the embryo was only 1.5 times higher than in the endosperm (including the aleurone) and that Se was quite evenly distributed throughout the whole of the grain. The Se distribution is very similar to that of sulphur (S) (see also Feeney *et al.*, 2003), which is not unexpected as these elements share the same mechanisms of uptake and transport (Hawkesford & Zhao, 2007), with *c.* 80% of the Se in the wheat grain being present in proteins as selenomethionine or selenocysteine (which replace methionine and cysteine, respectively) (Whanger, 2002).

Higher magnification images of the aleurone cell and starchy endosperm cells from the areas indicated by the boxes in Fig. 2 are shown in Figs 3a and b, respectively. These images were taken under the same analytical conditions so the Se ion counts can be quantitatively compared. The line scan of Fig. 3c indicates that the concentration of Se is greater inside the aleurone cell than in the surrounding region but that the distribution within the cell is relatively uniform. Figs 3b and d show that Se is concentrated in the protein region surrounding the starch granules in the starchy endosperm cells, with little signal detected inside the

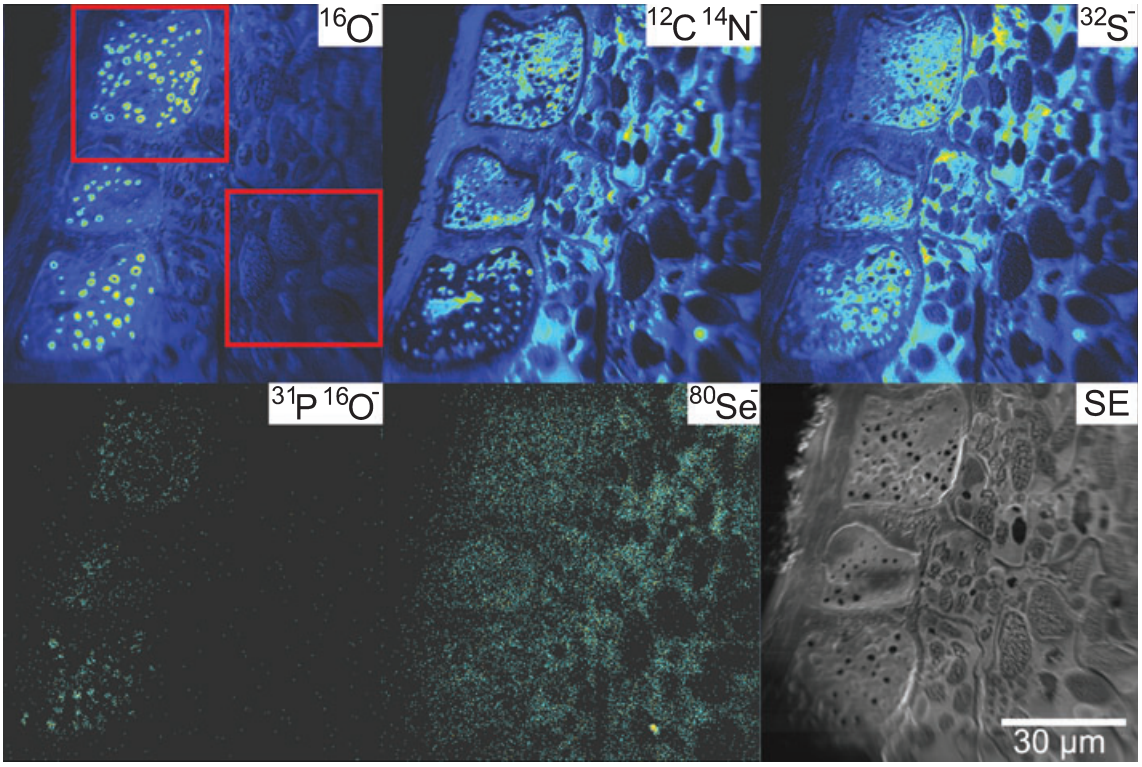

Fig. 2 NanoSIMS ion maps of the outer part of the wheat (*Triticum aestivum*) grain showing the distribution of $^{16}O^-$, $^{12}C^{14}N^-$, $^{32}S^-$, $^{31}P^{16}O^-$, $^{80}Se^-$ and secondary electron (SE) signals. An aleurone cell and a region of the starchy endosperm are indicated by red boxes and are presented at higher magnification in Figs 3a and b, respectively.

starch granules. Figs 3b and d also show that Se follows the S distribution.

The wheat grain sections prepared by high-pressure freezing were analysed under similar conditions to ensure that no artefacts had been introduced by the sample preparation method. Supporting Information Fig. S1 shows an aleurone cell, clearly showing phytate granules and the nucleus in the centre of the image. The morphology and chemical distribution is very similar to that shown in Fig. 3a. It can therefore be concluded that sectioning with a razor blade and removal of the platinum coating have not had a serious effect on the morphology or major element distribution in these samples.

The high-resolution capability of the NanoSIMS is illustrated in Fig. 4. This image together with Fig. 3d clearly shows that there is normally a close relationship between the distributions of S and Se at the submicron level. However, higher resolution imaging of the aleurone cells revealed the presence of 1–2 µm sized Se-rich areas as shown in Fig. 5. These regions appear to be situated on the outside of the phytate granules. Surprisingly, the same hotspots are not seen in the S map, with less S detected in these hotspots in comparison to the surrounding areas. In the other regions of the cell, the distribution of the Se follows closely that of S. Wheat is relatively tolerant to high concentrations of Se (Lyons *et al.*, 2005b) and it is possible that the wheat grain stores the Se in these localized regions, which may be vacuoles, to prevent high Se concentrations having toxic effects more widely within the grain. This is the first time that localization of Se to this kind of feature has been observed in the wheat grain and further work is needed to identify the processes that lead to this apparent sequestration. It would be interesting to investigate if the Se hotspots also occur in grain containing lower concentrations of Se, although analytically this will be difficult. Analysis of similarly Se-fertilized grains by high-performance liquid chromatography (HPLC)-ICP-MS showed little difference in the form of Se between the bran and white flour fractions; both contained selenomethionine as the major Se compound (Dave Hart, Institute for Food Research, Norwich, pers. comm.). It is therefore not clear what the likely form of Se is within these Se hotspots.

In Fig. 4 the $^{31}P^{16}O^-$ signal was more concentrated inside the starch grains and is presumably associated with phospholipids present within the starch granules. The characteristic 'porous' structure observed inside all of the starch grains, and shown most clearly in the $^{31}P^{16}O^-$ image of Fig. 4, is an artefact created by scanning the sectioned starch surface with an intense ion beam. The effect of ion beam milling has been confirmed with experiments in a

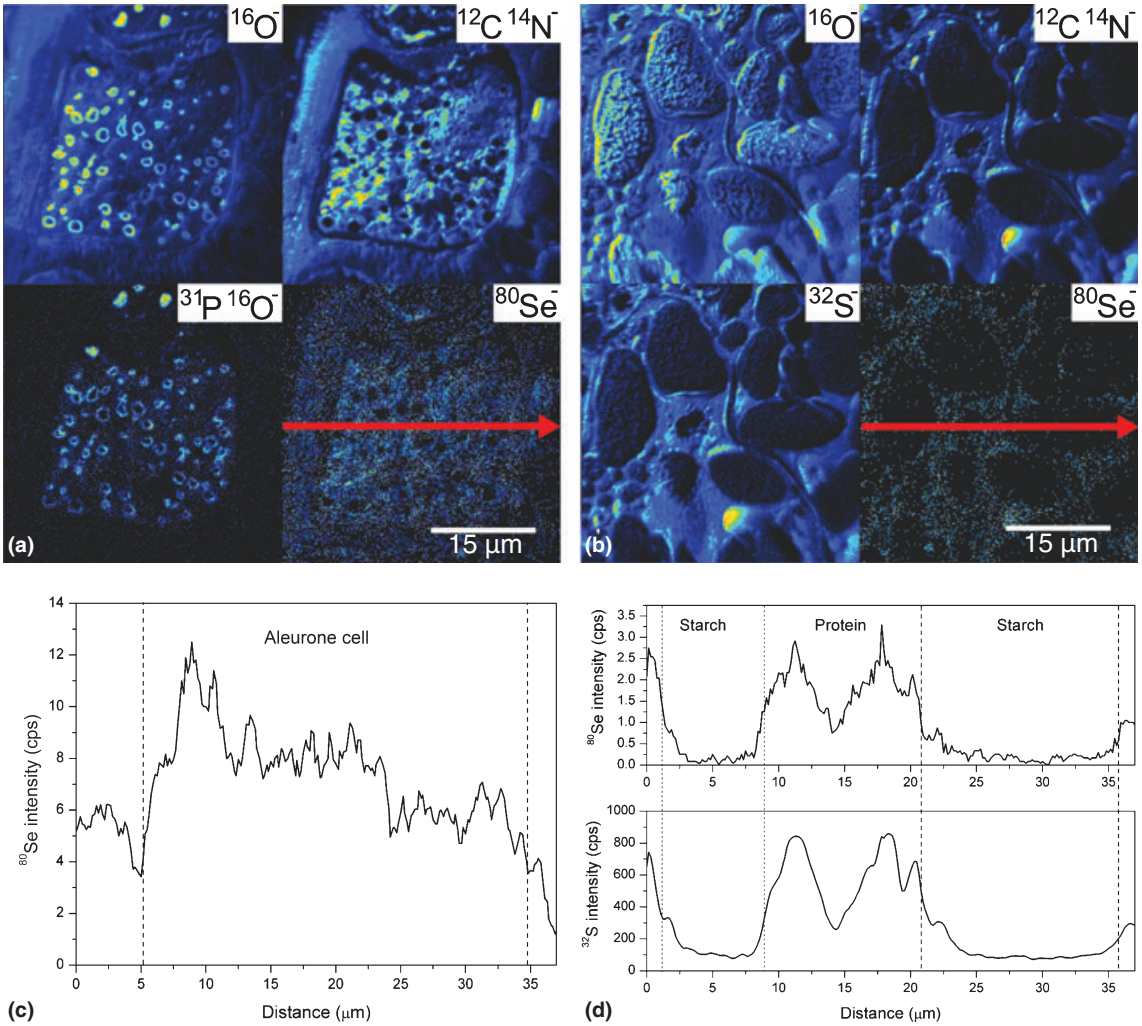

Fig. 3 Higher magnification NanoSIMS ion maps of (a) the wheat (*Triticum aestivum*) aleurone cell indicated in Fig. 2 showing $^{16}O^-$, $^{12}C^{14}N^-$, $^{31}P^{16}O^-$ and $^{80}Se^-$ signals, and (b) the wheat starchy endosperm region indicated in Fig. 2 showing $^{16}O^-$, $^{12}C^{14}N^-$, $^{32}S^-$ and $^{80}Se^-$ signals. (c) Line scan for $^{80}Se^-$ across the wheat aleurone cell as indicated by the arrow in (a), with the intensity in counts per second (cps). (d) Line scan for $^{80}Se^-$ and $^{32}S^-$ ions across the starchy endosperm region as indicated by the arrow in (b), with the intensity in cps. The line scans were averaged over 400 pixels to improve the counting statistics using a box with a width of 10 pixels (parallel to the line) and a height of 40 pixels (normal to the line) and stepped along the image in 1.5-µm intervals.

focused ion beam microscope which produced identical topographic features. These same features were also observed in wheat grain containing 100% amylopectin starch, suggesting that these characteristic features are a general response of starch on exposure to an energetic incident ion beam rather than preferential removal of different starch components.

Arsenic distribution in rice grains

Figure 6 is a low-magnification NanoSIMS image of the edge of a rice grain showing two aleurone cells and part of the starchy endosperm. The structure of the rice grain has been described diagrammatically by Krishnan & Dayanandan (2003). The structures and elemental distributions are very similar to those seen in the wheat grain, with the protein matrix around the starch granules in the starchy endosperm cells revealed by the characteristic distributions of the $^{12}C^{14}N^-$ and $^{32}S^-$ signals. It can be seen in this image that the As is concentrated in the protein matrix of the starchy endosperm cells just below the aleurone layer (the subaleurone) with very few counts from the aleurone layer itself. This pattern is also observed further into the grain, with the As being concentrated in the protein matrix. The concentration of protein decreases from the subaleurone cells to the central starchy endosperm cells and a similar gradient in As concentration is observed. Similar gradients in protein concentration have been demonstrated in endosperms of other cereal species (Tosi *et al.*, 2009). This finding may indicate that As is associated with thiol groups of the proteins.

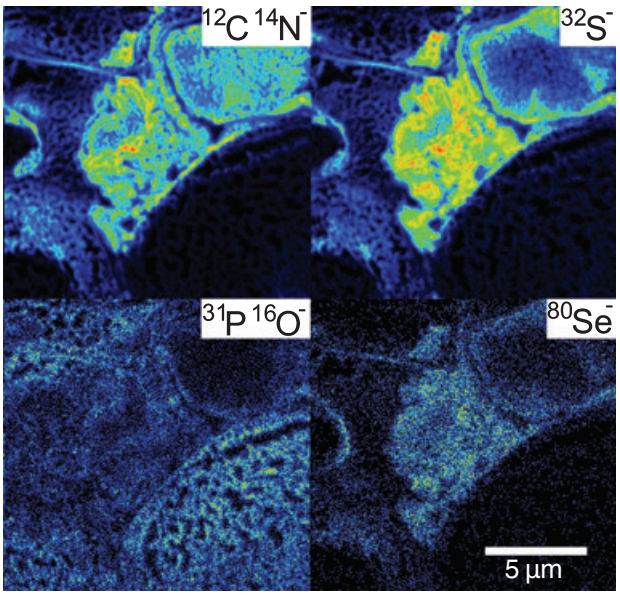

Fig. 4 High-resolution NanoSIMS ion maps of a proteinaceous region between the starch granules in the starchy endosperm cells of the wheat (*Triticum aestivum*) grain showing the distributions of the $^{12}C^{14}N^-$, $^{32}S^-$, $^{31}P^{16}O^-$ and $^{80}Se^-$ signals.

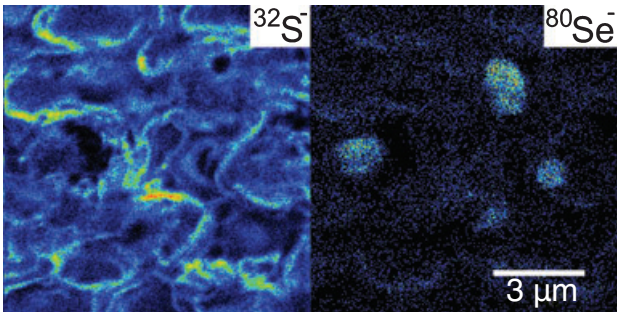

Fig. 5 High-resolution NanoSIMS ion maps from the middle of a wheat (*Triticum aestivum*) aleurone cell showing the $^{32}S^-$ and $^{80}Se^-$ signals. Selenium-rich hotspots are clearly observed but there are no accompanying sulphur hotspots.

Recently, Lombi *et al.* (2009) showed an S distribution in rice grains that decreased from the outer parts of the grain to the interior of the endosperm. Furthermore, As(III)-thiol complexes were found to represent over 50% of the total As in the endosperm of rice. Both these findings, obtained by particle induced X-ray emission (PIXE) and synchrotron techniques and therefore only resolved at the micron scale level, are corroborated by our results at the subcellular level.

The As speciation in similar samples was previously determined to be 30% inorganic As (mainly arsenite) and 70% dimethylarsinic acid (DMA) (Xu *et al.*, 2008). The presence of As(III)-thiolate complexes could not be revealed using the technique employed by Xu *et al.* (2008) but is likely considering the report of Lombi *et al.* (2009). This may explain why the distribution of the As is different to that of P because very little of the As in the rice grain is in the form of arsenate, which is chemically similar to phosphate. Transport of arsenite and DMA from vegetative tissues to the rice grain would thus be expected to follow a different pathway from that for phosphate (Zhao *et al.*, 2009).

Higher magnification images, taken under the same analytical conditions, enabled a direct comparison of the concentrations of key elements in the aleurone and starchy endosperm cells (Figs 7a and b, respectively). The ring structures in the $^{16}O^-$, $^{31}P^{16}O^-$ images and the dark circles in the secondary electron image of Fig. 7a correspond to the location of the phytate granules and are similar to the images of phytate in wheat reported by Heard *et al.* (2002), and are also similar to the $^{16}O^-$ and $^{31}P^{16}O^-$ maps in wheat (Figs 2, 3a). It was expected that the whole of the phytate granule would show a high concentration of P and O, but $^{16}O^-$, $^{31}P^{16}O^-$ signals were lacking from the central region of the granule, possibly because of an artefact from the well-known matrix effect in SIMS analysis (Benninghoven *et al.*, 1987; Wilson *et al.*, 1989). The yields of $^{16}O^-$ and $^{31}P^{16}O^-$ secondary ions are very low from the bulk of the phytate granules even though the local concentrations of these elements are high. The yields of these same ions adjacent to the surrounding material (matrix) are much higher and this leads to the ring structure. FIB imaging and energy dispersive X-ray spectroscopy demonstrated that these phytate granules have not been preferentially sputtered away to leave a hole and do indeed contain high concentrations of P and O. The majority of the phytate granules in Fig. S1 do not show the ring artefact, and it is possible that the presence of the underlying silicon wafer in these thin sections either increases the yield from the central region of the phytate granules or reduces the build-up of charge inside the granules (as proposed by Heard *et al.*, 2002). Unfortunately, this imaging artefact prevents the determination of the As content of the central regions of the phytate granules in the grains sectioned with a razor blade.

Line scans taken across the As images in Fig. 7 show that micron-scale regions of the starchy endosperm cells contain higher concentrations of As than the aleurone cells (Fig. 7c). If the As signal intensity from the starchy endosperm region (summed over that defined in Fig. 7a) is directly compared with that from the aleurone region, and it is assumed that there are no differential matrix effects in these two regions, it appears that there is a concentration of As 2.5 times higher in the starchy endosperm cells than in the aleurone cells. However, although the images were taken under very similar analytical conditions, there is a considerable difference in the intensity of the $^{12}C^{14}N^-$ signal (not shown in Fig. 7a) between the two images. For biological materials the $^{12}C^{14}N^-$ intensity is known to be very sensitive to topography, local matrix effects and protein-rich regions and so can be used to normalize other signals to at least partially remove these counting artefacts (Follet-Gueye

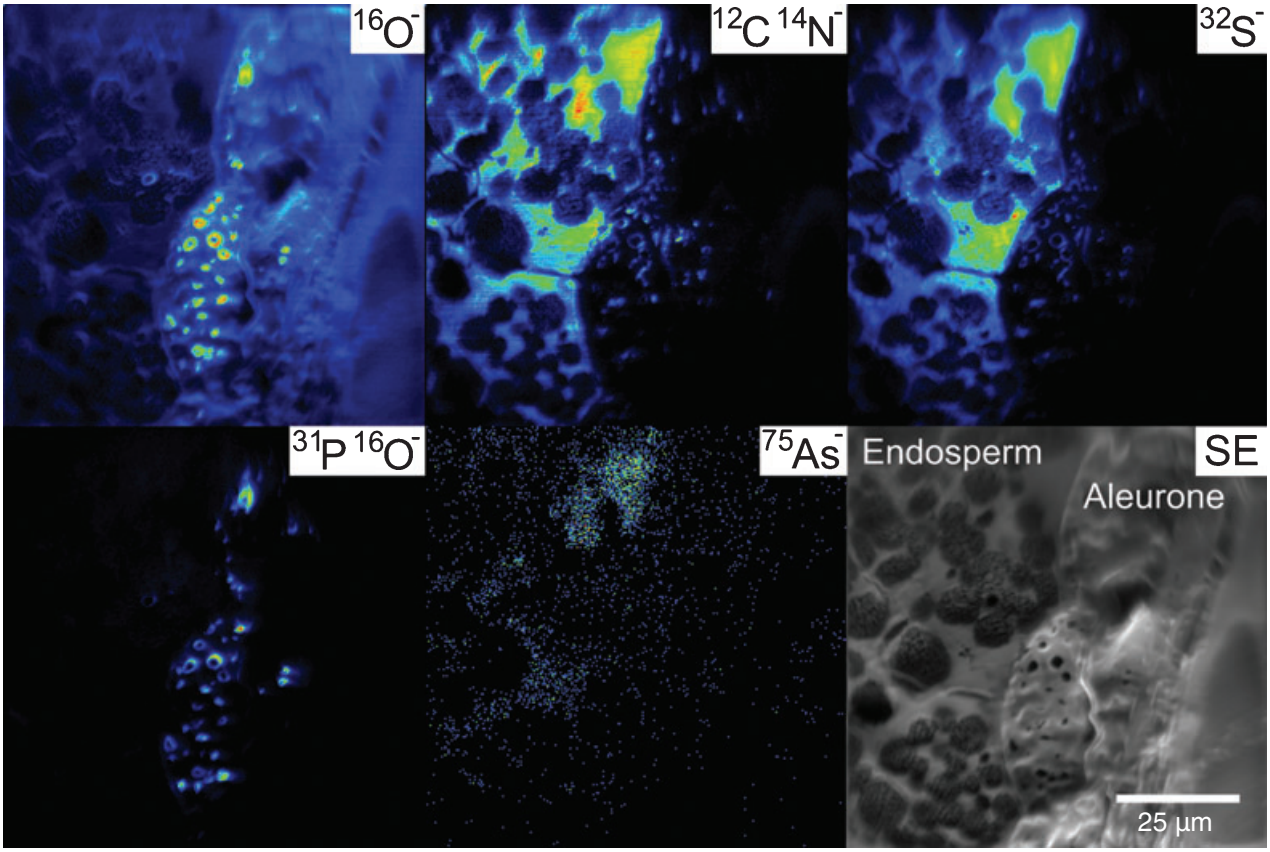

Fig. 6 NanoSIMS ion maps of the edge of a rice (*Oryza sativa*) grain showing the $^{16}O^-$, $^{12}C^{14}N^-$, $^{32}S^-$, $^{31}P^{16}O^-$, $^{75}As^-$ and secondary electron (SE) signals.

et al., 1998; Derue *et al.*, 2006). To take into account the chemical environment and topography differences between the two As images, the $^{75}As^-$ signal intensity was first normalized pixel by pixel with respect to the $^{12}C^{14}N^-$ signal and then ratioed. This increases the count ratio between the two regions to 18 in favour of the endosperm, suggesting an even greater difference in As concentration between the starchy endosperm and aleurone regions. When the As signal was normalized with the $^{32}S^-$ signal this gave a ratio of 5.8. It is currently not clear which of these values represents the closest approximation to the real compositional variation, but for all three estimates the As concentration is higher in the endosperm than in the aleurone cells.

Polishing of rice grains usually removes both the aleurone and the subaleurone layers and thus reduces the amount of As consumed via the rice grain. An unfortunate consequence of this processing is a depletion of protein, which could have consequences for nutrition in regions where rice provides a significant proportion of the daily protein intake. The bran and subaleurone cells also contain high concentrations of other beneficial components in addition to proteins (dietary fibre, vitamins, micronutrients and phytochemicals) which are lost by polishing (Lombi *et al.*, 2009).

In the sample analysed with S-XRF, As was localized near the ovular trace and nucellar projection (see Fig. S2). Because of the thickness of the sample required for NanoSIMS analysis, and penetration of the X-ray beam, the As map is somewhat distorted, but the main aim of using this technique, which has already been extensively used to analyse the localization of As in rice grains (Meharg *et al.*, 2008; Lombi *et al.*, 2009), was to target regions showing different As intensities for subsequent analysis with the NanoSIMS at higher resolution. At each location a 90 by 90 µm map (with a dwell time of 10 ms and a current of 29 pA) was obtained to compare the As distribution directly with the S-XRF data. Both optical and SEM examination indicated that the synchrotron beam was quite damaging to the rice sample as approximately every 15 µm there was a 1–2 µm sized hole. Ideally NanoSIMS analysis should be performed on a flat surface, but the presence of these holes was clear in the 90-µm scans and any enhancements of ion signals from these regions were disregarded.

In the regions near the ovular vascular trace and the nucellar projection, S-XRF showed a higher average As concentration and NanoSIMS analysis was able to identify micron-sized hotspots as shown in a typical image in Fig. 8

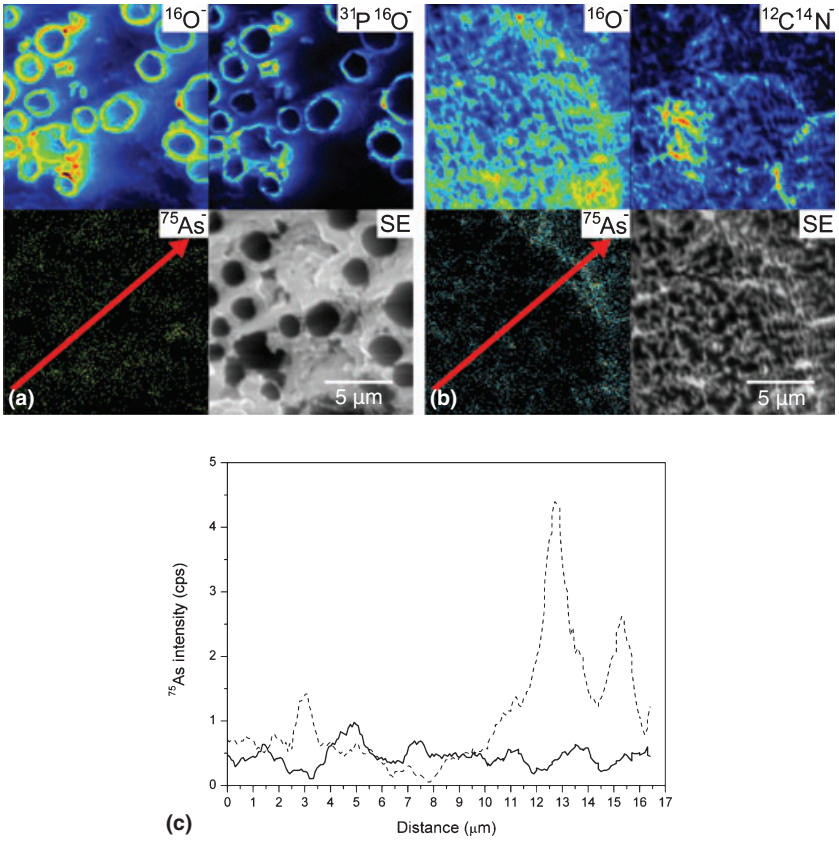

Fig. 7 High-magnification NanoSIMS ion maps of (a) a rice (*Oryza sativa*) aleurone cell showing $^{16}O^-$, $^{31}P^{16}O^-$, $^{75}As^-$ $^{80}Se^-$ signals and the secondary electron image, and (b) the rice starchy endosperm cell region showing $^{16}O^-$, $^{12}C^{14}N^-$, $^{75}As^-$ signals and the secondary electron image. (c) Arsenic intensity scans across the aleurone (solid line) and starchy endosperm (dashed line) images shown by the arrows in (a) and (b), respectively.

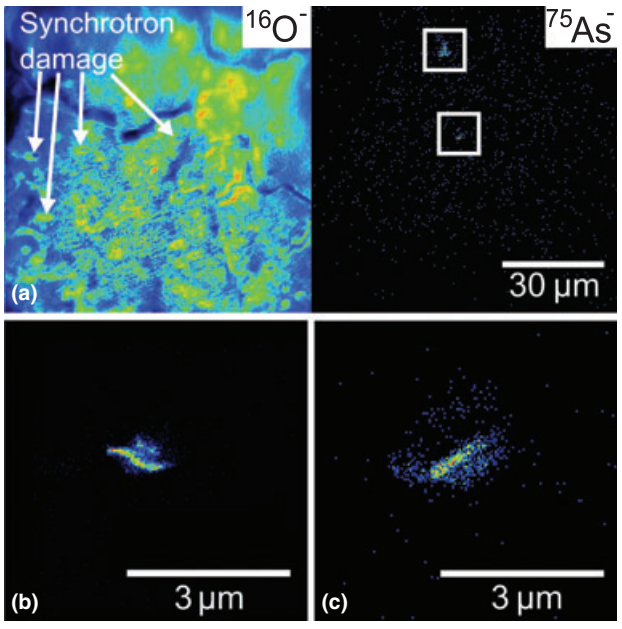

Fig. 8 (a) 90-µm NanoSIMS ion maps of rice (*Oryza sativa*) grain area 1 on Supporting Information Fig. S2 showing the $^{16}O^-$ (left panel) and $^{75}As^-$ (right panel) signals. Two arsenic (As) hotspots were found in this area. Higher magnification scans (10 µm) were taken of each of these; the upper hotspot is shown in (b) and the lower in (c). Synchrotron damage (regular holes) can be seen in the $^{16}O^-$ map.

(area 1 of Fig. S2). Hotspots were found in areas 1–4, 7 and 11–13 of Fig S2, and, in general, one or two hotspots were found in each 90-µm scan. With the exception of areas 7 and 13, no hotspots were found at any location other than the high-As region shown by S-XRF near the ovular vascular trace and nucellar projection. The ovular vascular trace, in conjunction with the chalazal and nucellar tissues, transports nutrients into the endosperm (Krishnan & Dayanandan, 2003). It is therefore not unexpected that there is a higher As concentration in this part of the grain. Because of the large step size of the S-XRF analysis it is possible that the highly localized hotspots in areas 7 and 13 lay between the analysis points, and hence these areas are shown in Fig. S2 as being low in As.

In each area analysed, the total number of As counts from NanoSIMS was normalized pixel by pixel with the total number of S counts in order to reduce errors caused by topography or small changes in primary ion current which could modify the yield of secondary ions. The normalized data were grouped into three regions, those near the ovular vascular trace and nucellar projection (the high-As region identified in the S-XRF data), aleurone and endosperm (all areas away from the high-As region), and averaged. Area 13 was excluded from the averages of the endosperm region because this area was anomalously high in both As and number of hotspots, as shown in Table S1.

Both the normalized data and the average number of hotspots per square micron (presented fully in Table S1) show that there is approximately twice as much As in the region near the ovular vascular trace and nucellar projection as in the endosperm, with no enrichment of As in the aleurone layer. The As:S ratio for the ovular vascular trace and nucellar projection region was $2.61 \times 10^{-4} \pm 1.5 \times 10^{-4}$, twice that of the endosperm As:S ratio of $1.37 \times 10^{-4} \pm 4.8 \times 10^{-5}$ (quoted errors are 1 SD). The As X-ray signal from the synchrotron data in the As-enriched region near the nucellar projection is approximately double that of the endosperm part of the grain, and hence there is good quantitative agreement in the ratio of As between the two regions from the two techniques.

The lateral resolution of the synchrotron analysis is not sufficient to show details of the localization of As in the As-rich areas. The combination of a large step size and large interaction volume means that several small hotspots may be included under one analysis point and therefore a high, but diffuse, As signal is presented in the synchrotron map. Furthermore, because of the penetration of the X-rays, hotspots of As located within the volume probed by the beam would also contribute to the measured signal. Therefore, if hotspots were located in the same area but at different depths the overall map would show a more homogeneous distribution of As. By contrast, SIMS is inherently a surface analysis technique and therefore the signal is generated only from the top few nanometers of the sample surface. With the higher resolution capabilities of the NanoSIMS, it is quite clear that the higher average As concentrations were actually located in small As hotspots near the ovular vascular trace and nucellar projection. At present it is not clear why the As is localized in these micron-sized hotspots.

Two recent papers have reported that rice bran contains high concentrations of As (Meharg *et al.*, 2008; Sun *et al.*, 2008). Meharg *et al.* (2008) suggest that the As is localized in the pericarp and aleurone, but the data presented here indicate subaleurone localization. The S-XRF images presented by Meharg *et al.* (2008) and Lombi *et al.* (2009) also clearly show a region of As localization at the surface, which is suggested to correspond with the surface longitudinal groove, and this is consistent with the new S-XRF and NanoSIMS data presented here.

In the supporting information of Meharg *et al.* (2008), a higher resolution S-XRF map is presented which shows As accumulation within *c.* 200 μm of the edge of the rice grain. Combining the NanoSIMS and S-XRF data presented in this paper and these higher resolution S-XRF data (Meharg *et al.*, 2008), a consistent explanation for why milling of the grain reduces the overall As concentration in the grain as stated by Ren *et al.* (2006) and Sun *et al.* (2008) can be suggested. In both of these papers the relative As concentrations in the different parts of the grain are calculated after separating the bran layer from the endosperm by milling or polishing. Franz & Sampson (2006) state that the bran layer comprises 7% of the mass of a whole rice grain, and Sun *et al.* (2008) used this value to indicate when polishing should be stopped. However, it is difficult to control this process so that only the aleurone layer is removed during polishing, and it is likely that part of the region immediately underneath the aleurone layer, the subaleurone, was also removed. Fig. 6 shows this subaleurone region to have a high As concentration. The data presented in a recent paper by Norton *et al.* (2009) are also consistent with As being localized in the subaleurone. In the paper by Sun *et al.* (2008), removal of 7% of the grain resulted in a 10% decrease in the As concentration; however, Norton *et al.* (2009) milled away 20% of the grain, which resulted in a 45% reduction in the As concentration. This more severe milling would presumably result in complete removal of the high-As subaleurone region and hence explain the marked decrease in As concentration. The NanoSIMS maps shown in Fig. 6, the combined synchrotron and NanoSIMS data of Fig. S2 and Fig. 8, the higher resolution S-XRF data of Meharg *et al.* (2008) and the milling data of Norton *et al.* (2009) consistently indicate that this subaleurone layer and possibly the ovular vascular trace contain the highest concentration of As, and explain why milling of the grain reduces the overall As concentration in these rice samples. It is also possible that rice embryos contain higher concentrations of As than other parts of the grain (embryos are removed during polishing) and this is an obvious target for future analysis using NanoSIMS.

Conclusions

This study has demonstrated that NanoSIMS is a powerful technique for identifying the location of important trace elements in cereal grains. To our knowledge, this is the first time the precise location of parts-per-million concentrations of Se and As have been analysed with subcellular resolution, and several new features have been observed.

This report demonstrates that in wheat Se is located relatively uniformly across the aleurone, apart from the presence of Se-rich hotspots, and also in the protein matrix surrounding the starch granules in the starchy endosperm. The similar distribution patterns of Se and S suggest that the two elements are transported to and deposited in the grain via the same pathway. The presence of the Se-rich hotspots in the aleurone cells is yet to be explained as there are no accompanying S hotspots.

In the rice samples far from the ovular vascular trace, As is more concentrated in the protein matrix in the subaleurone cells of the endosperm with very little in the aleurone layer. Near the ovular vascular trace and nucellar projection the macroscopic variation in As revealed by the S-XRF

experiment is a result of increased concentrations of micron-sized As-rich regions. These patterns are in contrast to that of P, suggesting that the two elements follow different pathways into the grain. It is believed this is the first time S-XRF and NanoSIMS analysis has been used on the same sample, and there is good quantitative agreement between the two techniques.

Acknowledgements

The authors would like to thank Dr Martin Broadley of Nottingham University for supplying the wheat grain samples, Dr Kirk Scheckel of the US EPA for assistance with the synchrotron measurements and Barry Martin at Oxford Brookes University and Cristina Gritsch at Rothamsted Research for preparation of the high-pressure frozen wheat grain sample. This work was supported by funding from UK EPSRC (grant no. GR/T19797). Rothamsted Research is an institute of the UK Biotechnology and Biological Sciences Research Council. PNC/XOR facilities at the Advanced Photon Source and research at these facilities are supported by the US Department of Energy – Basic Energy Sciences, a major facilities access grant from NSERC, the University of Washington, Simon Fraser University and the Advanced Photon Source. Use of the Advanced Photon Source is also supported by the US Department of Energy, Office of Science, Office of Basic Energy Sciences, under Contract DE-AC02-06CH11357.

References

Audinot JN, Schneider S, Yegles M, Hallegot P, Wennig R, Migeon HN. 2004. Imaging of arsenic traces in human hair by Nano-SIMS 50. *Applied Surface Science* **231–2**: 490–496.

Benninghoven A, Reudenauer FG, Werner HW. 1987. *Secondary ion mass spectrometry: basic concepts, instrumental aspects, applications, and trends*. New York, NY, USA: John Wiley.

Broadley MR, White PJ, Bryson RJ, Meacham MC, Bowen HC, Johnson SE, Hawkesford MJ, McGrath SP, Zhao FJ, Breward N *et al.* 2006. Biofortification of UK Food Crops with Selenium. *Proceedings of the Nutrition Society* **65**: 169–181.

Burns MS. 1982. Applications of secondary ion mass-spectrometry (SIMS) in biological research: a review. *Journal of Microscopy-Oxford* **127**: 237–258.

Chandra S, Morrison GH. 1992. Sample preparation of animal-tissues and cell-cultures for secondary ion mass-spectrometry (SIMS) microscopy. *Biology of the Cell* **74**: 31–42.

Chandra S, Smith DR, Morrison GH. 2000. Subcellular imaging by dynamic SIMS ion microscopy. *Analytical Chemistry* **72**: 104a–114a.

Combs GF. 2001. Selenium in global food systems. *British Journal of Nutrition* **85**: 517–547.

Derue C, Gibouin D, Demarty M, Verdus MC, Lefebvre F, Thellier M, Ripoll C. 2006. Dynamic-SIMS imaging and quantification of inorganic ions in frozen-hydrated plant samples. *Microscopy Research and Technique* **69**: 53–63.

Eurola M, Ekholm P, Ylinen M, Koivistoinen P, Varo P. 1991. Effects of selenium fertilization on the selenium content of cereal-grains, flour, and bread produced in Finland. *Cereal Chemistry* **67**: 334–337.

Feeney KA, Heard PJ, Zhao FJ, Shewry PR. 2003. Determination of the distribution of sulphur in wheat starchy endosperm cells using secondary ion mass spectrometry (SIMS) combined with isotope enhancement. *Journal of Cereal Science* **37**: 311–318.

Follet-Gueye M-L, Verdus M-C, Demarty M, Thellier M, Ripoll C. 1998. Cambium pre-activation in beech correlates with a strong temporary increase of calcium in cambium and phloem but not in xylem cells. *Cell Calcium* **24**: 205–211.

Fordyce FM, Zhang GD, Green K, Liu XP. 2000. Soil, grain and water chemistry in relation to human selenium-responsive diseases in Enshi District, China. *Applied Geochemistry* **15**: 117–132.

Franz M, Sampson L. 2006. Challenges in developing a whole grain database: definitions, methods and quantification. *Journal of Food Composition and Analysis* **19**: 38–44.

Grignon N, Halpern S, Gojon A, Fragu P. 1992. N-14 and N-15 imaging by SIMS microscopy in soybean leaves. *Biology of the Cell* **74**: 143–146.

Grovenor CRM, Smart KE, Kilburn MR, Shore B, Dilworth JR, Martin B, Hawes C, Rickaby REM. 2006. Specimen preparation for NanoSIMS snalysis of biological materials. *Applied Surface Science* **252**: 6917–6924.

Grundas ST. 2003. Wheat | grain structure of wheat and wheat-based products. In: Caballero B, Trugo LC, Finglas PM, eds. *Encyclopedia of food sciences and nutrition*. Oxford, UK: Academic Press, 6137–6146.

Guerquin-Kern JL, Wu TD, Quintana C, Croisy A. 2005. Progress in analytical imaging of the cell by dynamic secondary ion mass spectrometry (SIMS microscopy). *Biochimica Et Biophysica Acta-General Subjects* **1724**: 228–238.

Hartikainen H. 2005. Biogeochemistry of selenium and its impact on food chain quality and human health. *Journal of Trace Elements in Medicine and Biology* **18**: 309–318.

Hawkesford MJ, Zhao FJ. 2007. Strategies for increasing the selenium content of wheat. *Journal of Cereal Science* **46**: 282–292.

Heard PJ, Feeney KA, Allen GC, Shewry PR. 2002. Determination of the elemental composition of mature wheat grain using a modified secondary ion mass spectrometer (SIMS). *Plant Journal* **30**: 237–245.

Krishnan S, Dayanandan P. 2003. Structural and histochemical studies on grain-filling in the caryopsis of rice (*Oryza sativa* L.). *Journal of Biosciences* **28**: 455–469.

Levi-Setti RR. 1988. Structural and microanalytical imaging of biological materials by scanning microscopy with heavy-ion probes. *Annual Review of Biophysics and Biophysical Chemistry* **17**: 325–347.

Lombi E, Scheckel KG, Pallon J, Carey AM, Zhu YG, Meharg AA. 2009. Speciation and distribution of arsenic and localization of nutrients in rice grains. *New Phytologist* **184**: 193–201.

Lyons GH, Genc Y, Stangoulis JCR, Palmer LT, Graham RD. 2005a. Selenium distribution in wheat grain, and the effect of postharvest processing on wheat selenium content. *Biological Trace Element Research* **103**: 155–168.

Lyons GH, Stangoulis JCR, Graham RD. 2005b. Tolerance of wheat (*Triticum aestivum* L.) to high soil and solution selenium levels. *Plant and Soil* **270**: 179.

Ma JF, Yamaji N, Mitani N, Xu X-Y, Su Y-H, McGrath SP, Zhao F-J. 2008. Transporters of arsenite in rice and their role in arsenic accumulation in rice grain. *Proceedings of the National Academy of Sciences, USA* **105**: 9931–9935.

Meharg AA, Rahman M. 2003. Arsenic contamination of Bangladesh paddy field soils: implications for rice contribution to arsenic consumption. *Environmental Science & Technology* **37**: 229–234.

Meharg AA, Lombi E, Williams PN, Scheckel KG, Feldmann J, Raab A, Zhu YG, Islam R. 2008. Speciation and localization of arsenic in white and brown rice grains. *Environmental Science & Technology* **42**: 1051–1057.

Norton GJ, Islam MR, Deacon CM, Zhao FJ, Stroud JL, McGrath SP, Islam S, Jahiruddin M, Feldmann J, Price AH *et al.* 2009. Identification of low inorganic and total grain arsenic rice cultivars

from Bangladesh. *Environmental Science & Technology* **43**: 6070–6075.

Quintana C, Bellefqih S, Laval JY, Guerquin-Kern JL, Wu TD, Avila J, Ferrer I, Arranz R, Patino C. 2006. Study of the localization of iron, ferritin, and hemosiderin in Alzheimer's disease hippocampus by analytical microscopy at the subcellular level. *Journal of Structural Biology* **153**: 42–54.

Rahman MA, Hasegawa H, Rahman MM, Miah MAM, Tasmin A. 2008. Arsenic accumulation in rice (*Oryza sativa* L.): human exposure through food chain. *Ecotoxicology and Environmental Safety* **69**: 317–324.

Rayman MP. 2002. The argument for increasing selenium intake. *Proceedings of the Nutrition Society* **61**: 203–215.

Ren X-L, Liu Q-L, Wu D-X, Shu Q-Y. 2006. Variations in concentration and distribution of health-related elements affected by environmental and genotypic differences in rice grains. *Rice Science* **13**: 170–178.

Schwarz K, Foltz CM. 1957. Selenium as an integral part of factor 3 against dietary necrotic liver degeneration. *Journal of the American Chemical Society* **79**: 3292–3293.

Smart KE, Kilburn MR, Salter CJ, Smith JAC, Grovenor CRM. 2007. NanoSIMS and EPMA analysis of nickel localisation in leaves of the hyperaccumulator plant *Alyssum lesbiacum*. *International Journal of Mass Spectrometry* **260**: 107–114.

Sun G-X, Williams PN, Carey A-M, Zhu Y-G, Deacon C, Raab A, Feldmann J, Islam RM, Meharg AA. 2008. Inorganic arsenic in rice bran and its products are an order of magnitude higher than in bulk grain. *Environmental Science & Technology* **42**: 7542–7546.

Tosi P, Parker M, Gritsch CS, Carzaniga R, Martin B, Shewry PR. 2009. Trafficking of storage proteins in developing grain of wheat. *Journal of Experimental Botany* **60**: 979–991.

Whanger PD. 2002. Selenocompounds in plants and animals and their biological significance. *Journal of the American College of Nutrition* **21**: 223–232.

Williams PN, Raab A, Feldmann J, Meharg AA. 2007. Market basket survey shows elevated levels of As in South Central US processed rice compared to California: consequences for human dietary exposure. *Environmental Science & Technology* **41**: 2178–2183.

Williams PN, Lombi E, Sun GX, Scheckel K, Zhu YG, Feng XB, Zhu JM, Carey AM, Adomako E, Lawgali Y *et al.* 2009. Selenium characterization in the global rice supply chain. *Environmental Science & Technology* **43**: 6024–6030.

Wilson RG, Stevie FA, Magee CW. 1989. *Secondary ion mass spectrometry: a practical handbook for depth profiling and bulk impurity analysis*. New York, NY, USA: Wiley.

Xu XY, McGrath SP, Meharg AA, Zhao FJ. 2008. Growing rice aerobically markedly decreases arsenic accumulation. *Environmental Science & Technology* **42**: 5574–5579.

Zhao FJ, Ma JF, Meharg AA, McGrath SP. 2009. Arsenic uptake and metabolism in plants. *New Phytologist* **181**: 777–794.

Supporting Information

Additional supporting information may be found in the online version of this article.

Fig. S1 High-resolution secondary ion mass spectrometry (NanoSIMS) ion maps of an aleurone cell from the high-pressure frozen wheat grain sample showing the $^{16}O^-$, $^{12}C^{14}N^-$, $^{31}P^{16}O^-$ and secondary electron signals.

Fig. S2 Synchrotron X-ray fluorescence (S-XRF) map of the top half of a transversely sectioned (As)-containing rice grain showing a high As concentration near the ovular vascular trace.

Table S1 Average of arsenic:sulphur (As:S) normalized high-resolution secondary ion mass spectrometry (NanoSIMS) data and average number of hotspots per square micron for the ovular vascular trace and nucellar projection (region of high As concentration), the endosperm, the aleurone and area 13

Please note: Wiley-Blackwell are not responsible for the content or functionality of any supporting information supplied by the authors. Any queries (other than about missing material) should be directed to the *New Phytologist* Central Office.